PCCP

ROYAL SOCIETY OF CHEMISTRY

PAPER

View Article Online
View Journal | View Issue

Check for updates

Cite this: *Phys. Chem. Chem. Phys.*, 2023, **25**, 13877

A general binary isotherm model for amines interacting with CO_2 and H_2O†

Yuta Kaneko * and Klaus S. Lackner *

Received 8th February 2023,
Accepted 20th April 2023

DOI: 10.1039/d3cp00624g

rsc.li/pccp

CO_2 capture by primary or secondary amines has been a topic of great research interests for a century because of its industrial importance. Interest has grown even more, because of the need to eliminate CO_2 emissions that lead to global warming. Experimental evidence shows that CO_2 sorption by primary or secondary amines is accompanied by co-absorption of H_2O. A quantitative analysis of such CO_2–H_2O co-absorption behavior is important for practical process design and theoretical understanding. Even though there is almost an experimental consensus that water enhances CO_2 uptake capacity, an analytical model to explain this phenomenon is not well established. Instead, some empirical models such as the Toth model are used to describe the isotherm without accounting for the presence of water. Recently, we have demonstrated that the isotherm equation of CO_2 sorption into strong-base anion exchange materials with quaternary ammonium can be derived from that of strong-base aqueous alkaline solutions by correcting for the drastic change in the water activity and by including an appropriate parameterization of the water activity terms. In this paper, we generalize this model from quaternary ammonium to primary, secondary and tertiary amines either in solutions or as functional groups in polymer resins. For primary, secondary and tertiary amines, the isotherm equation can be derived by extending that of a weak-base aqueous alkaline solution such as aqueous ammonia. The model has been validated using experimental data on CO_2 sorption for aqueous ammonia from the literature. This general model even includes quaternary ammonium as a special limit. Hence, this general model offers a platform that can treat the isotherms of solid amines, aqueous amines and aqueous alkaline solutions in a unified manner.

1 Introduction

CO_2 absorption into primary, secondary or tertiary amines has been investigated for a century because of their industrial importance and scientific interest. From an industrial point of view, the basic process of CO_2 scrubbing from flue gas using aqueous amines was patented as early as 1930.[1,2] Shortly after, Gregory and Scharmann (1937) from Standard Oil Company of Louisiana and Standard Oil Development Company presented experimental pilot plant data on CO_2 scrubbing using primary, secondary and tertiary amines (monoethanolamine, diaminoisopropanol and triethanolamine, respectively) from hydrogenation process gas.[3] From a theoretical perspective, the basic mechanism of CO_2 absorption into primary, secondary and tertiary amines has been proposed by researchers such as Goodridge (1955),[4] Danckwerts (1979)[5] and Donaldson and Nguyen (1980).[6]

Since the comprehensive investigations by these pioneers, many researchers have pointed out an interesting, experimentally observed feature of this sorption system: the CO_2 sorption in primary or secondary amines is accompanied by the co-absorption of H_2O.[4,7] Today, there is a general consensus among experimentalists that the presence of water enhances the CO_2 uptake capacity of these sorbents. However, an isotherm equation that explicitly includes the influence of water has not yet been derived from the governing equations. Instead, some empirical models such as the Toth model[8] have been used for CO_2 sorption isotherms for amine-functionalized silica, cellulose, and commercially-available weakly basic anion exchange resins such as Lewatits® VP OC 1065 in previous research, all of which contain primary, secondary or tertiary amines.[9–12] The Toth model is an empirical extension of the Langmuir isotherm, which improves the fit both at low and high pressures.[8] The impact of water on the CO_2 isotherm is only captured by fitting parameters that vary with the water vapor pressure over the sorbent.

On the other hand, a strong-base anion exchange material (AEM) with quaternary ammonium in a hydroxide–carbonate–bicarbonate form can also bind with CO_2 through a chemical reaction with hydroxide ions. In the 2000s, it was experimentally

School of Sustainable Engineering & the Built Environment, Arizona State University, Tempe, AZ 85287, USA. E-mail: ykaneko1@asu.edu, Klaus.Lackner@asu.edu

† Electronic supplementary information (ESI) available. See DOI: https://doi.org/10.1039/d3cp00624g

observed that the CO_2 affinity of a strong-base anion exchange resin is affected by humidity levels, which points to the presence of moisture-swing or moisture-controlled CO_2 sorption.[13–16] In this system, CO_2 is sorbed when the sorbent is dry, and CO_2 is desorbed when the sorbent is wet.[17–19] Interestingly, such a negative correlation between water and CO_2 sorption in quaternary ammonium is opposite to co-absorption observed in primary amines or secondary amines. In a previous paper, we demonstrated that the CO_2 isotherm equation of a strong-base AEM can be derived by extending the theory of strong-base aqueous alkaline solutions.[20,21] The resulting isotherm equation explicitly includes the water concentration term and thus can quantitatively account for the influence of water. The model predicts that increasing the humidity of the surrounding gas results in the deviation from the Langmuir isotherm, which has been validated using literature data. Analogously, we hypothesize here that the deviation of CO_2 sorption isotherms of primary, secondary and tertiary amines from the Langmuir isotherm could be explained analytically in terms of the governing equations instead of adopting empirical models such as the Toth model.

In this paper, we extend the concepts we applied to moisture-controlled strong base AEMs to AEMs functionalized with primary, secondary and tertiary amines. The model also describes aqueous 0solutions of these amines, as well as ammonia. Therefore, in the next section, we briefly review the chemistry of CO_2—amine systems to clarify the differences in CO_2 capture mechanisms among primary amines, secondary amines, tertiary amines and quaternary ammonium. In the theory section of this paper, all of these cases are unified into a single general model. In the result section, we validate this model using the experimental data on CO_2 sorption for aqueous ammonia from the literature.

2 Review of CO_2 capture mechanism

We begin by reviewing the mechanisms for CO_2 capture in different amine configurations. For primary and secondary amines, sorption can occur in a nearly water-free environment, but water will strongly influence the reaction pathways. For tertiary amines, all possible reactions require the presence of water. Quaternary ammonium sorption also involves water.

2.1 CO_2 capture by primary, secondary and tertiary amines

The chemical reaction of CO_2 with primary amines (RNH_2) comprises two sequential elementary reactions.[5,16] The first step leads to the formation of carbamic acids (RNHCOOH) as:

$$CO_2 + RNH_2 \rightleftharpoons RNHCOOH \quad (1)$$

In an aqueous environment, the carbamic acid is almost completely dissociated into $RNHCOO^-$ and H^+[6] as:

$$RNHCOOH \rightleftharpoons RNHCOO^- + H^+ \quad (2)$$

This proton is picked up by another primary amine, causing the second reaction that forms ammonium carbamate ion pairs ($RNHCOO^- + RNH_3^+$) as:[5,6]

$$RNHCOOH + RNH_2 \rightleftharpoons RNHCOO^- + RNH_3^+ \quad (3)$$

or,

$$H^+ + RNH_2 \rightleftharpoons RNH_3^+ \quad (4)$$

Although this paper is focused on equilibrium considerations and not kinetics, it has been observed in the literature that eqn (1) is the rate-limiting step and eqn (4) occurs instantly.[5,6] The overall reaction is

$$CO_2 + 2RNH_2 \rightleftharpoons RNH_3^+ + RNHCOO^- \quad (5)$$

This overall equation indicates that the sorption of a CO_2 molecule requires two amine molecules: one to bind the CO_2 molecule to the amine to form a carbamate ion, and the second to balance charge and bind with the proton produced in the process by forming an ammonium ion. It is well-known that humidity enhances the CO_2 uptake by supported amine materials and increases their amine efficiency.[11] In order to account for this mechanism, it has been pointed out that the following reaction may occur additionally to convert the carbamate ions into bicarbonate ion in the presence of water:[4,7]

$$RNHCOO^- + 2H_2O + CO_2 \rightleftharpoons RNH_3^+ + 2HCO_3^- \quad (6)$$

This indicates that water enhances CO_2 sorption into primary amines. Under this condition, theoretical maximum sorption efficiency increases to one CO_2 molecule per nitrogen atom.

Essentially the same discussions as presented above apply to secondary amines with the only difference being the replacement of RH with RR′ in eqn (1) through eqn (6). However, in tertiary amines, CO_2 capture under anhydrous conditions does not occur because the tertiary amines do not have a proton to give.[4] Therefore, tertiary amines can capture CO_2 only by catalyzing the formation of bicarbonate according to the following chemical reaction:[6,22]

$$CO_2 + RR'R''N + H_2O \rightleftharpoons RR'R''NH^+ + HCO_3^- \quad (7)$$

Namely, tertiary amines require water to capture CO_2.

2.2 CO_2 capture by quaternary ammonium

The properties and usage of quaternary ammonium are significantly different from those of primary, secondary and tertiary amines mainly because quaternary ammonium cannot release a proton and thus is always positively charged. Quaternary ammonium has been widely used in AEM membranes for electrodialysis or fuel cells. When the counterion to the quaternary ammonium is a hydroxide ion, CO_2 reacts with the hydroxide and can be captured/released through the following chemical reactions:[18,19]

$$CO_2 + OH^-(H_2O)_z \rightleftharpoons HCO_3^-(H_2O)_x + n_1H_2O \quad (8)$$

$$HCO_3^-(H_2O)_x + OH^-(H_2O)_z + n_2H_2O \rightleftharpoons CO_3^{2-}(H_2O)_y \quad (9)$$

where,

$$n_1 = -x + z \quad (10)$$

$$n_2 = -x + y - z - 1 \quad (11)$$

Note that x, y and z denote the number of hydration water molecules bound to each counterion, HCO_3^-, CO_3^{2-} and OH^-, respectively. Keeping track of the total water is important in explaining the moisture effect on CO_2 sorption. At a partial pressure of 40 Pa of CO_2 the relative humidity strongly affects the equilibrium loading of the strong-base ion exchange material. Finally, these chemical reactions indicate that the theoretical maximum amine efficiency is 0.5 when quaternary ammonium in a carbonate–bicarbonate form is used as moisture-controlled CO_2 sorbents.

2.3 Difference among quaternary ammonium and primary/secondary/tertiary amines

There are mainly two differences between quaternary ammonium and other amines. One is that primary and secondary amines not only catalyze hydration of CO_2 but also directly capture CO_2 to form carbamate while tertiary amines and quaternary ammonium capture CO_2 only by catalyzing hydration of CO_2. Even though primary and secondary amines need no water for capturing CO_2, their affinity to CO_2 is nevertheless profoundly affected by the presence of water. The other difference is that the base dissociation constant K_b needs to be introduced for weak-bases such as primary, secondary and tertiary amines. Hence, we start with an isotherm theory of aqueous ammonia to construct a general model. This is similar to the approach adopted for understanding strong-base anionic exchange resins in a previous study by Kaneko and Lackner (2022a).[20]

3 Theory

In this paper, we will account for all the chemical species and their transitions, but will not assume a specific relationship between water in the sorbent and the surrounding water vapor, because it will vary from material to material. For example, the Flory–Huggins theory will apply to water absorption into anion exchange materials.[23,24] Further work on specific sorbents is required to elucidate the water isotherm of a specific model.

3.1 Isotherm equation for aqueous ammonia

In aqueous ammonia, the following nine equations apply simultaneously:[25]

$$H_2O_{(g)} \overset{K_{H(H_2O)}}{\rightleftharpoons} H_2O_{(aq)} \quad (12)$$

$$CO_{2(g)} \overset{K_{H(CO_2)}}{\rightleftharpoons} CO_{2(aq)} \quad (13)$$

$$NH_{3(g)} \overset{K_{H(NH_3)}}{\rightleftharpoons} NH_{3(aq)} \quad (14)$$

$$NH_{3(aq)} + CO_2 \overset{K_X}{\rightleftharpoons} NH_2COOH \quad (15)$$

$$NH_2COOH + OH^- \overset{K_Y}{\rightleftharpoons} H_2O + NH_2COO^- \quad (16)$$

$$NH_{3(aq)} + H_2O_{(aq)} \overset{K_b}{\rightleftharpoons} NH_4^+ + OH^- \quad (17)$$

$$CO_{2(aq)} + OH^- \overset{K_1}{\rightleftharpoons} HCO_3^- \quad (18)$$

$$HCO_3^- + OH^- \overset{K_2}{\rightleftharpoons} CO_3^{2-} + H_2O_{(aq)} \quad (19)$$

$$H_2O_{(aq)} \overset{K_W}{\rightleftharpoons} H^+ + OH^- \quad (20)$$

where, apparent equilibrium coefficients and Henry's constants are defined as:

$$K_{H(CO_2)} \equiv \frac{[CO_2]}{P_{CO_2}} \quad (21)$$

$$K_{H(NH_3)} \equiv \frac{[NH_3]}{P_{NH_3}} \quad (22)$$

$$K_X \equiv \frac{[NH_2COOH]}{[NH_3][CO_2]} \quad (23)$$

$$K_Y \equiv \frac{[NH_2COO^-]}{[NH_2COOH][OH^-]} \quad (24)$$

$$K_b \equiv \frac{[NH_4^+][OH^-]}{[NH_3]} \quad (25)$$

$$K_1 \equiv \frac{[HCO_3^-]}{[CO_2][OH^-]} \quad (26)$$

$$K_2 \equiv \frac{[CO_3^{2-}]}{[HCO_3^-][OH^-]} \quad (27)$$

$$K_W \equiv [H^+][OH^-] \quad (28)$$

Note that i in brackets as in $[i]$ represents the concentration of the chemical species i. K_b denotes the base dissociation constant of ammonia in aqueous solutions. Later, we will generalize the isotherm model for aqueous ammonia to weak acids such as amino acids or amphoteric compounds such as primary amines. For these compounds, the values of the acid dissociation constant, K_a, have been well investigated and are available in the literature rather than K_b. Therefore, it is convenient to translate K_b to K_a or pK_a using the equation:

$$pK_a + pK_b = pK_W \quad (29)$$

According to the literature the values of these equilibrium coefficients at 25 °C are given as:[26–32]

$$K^\circ_{H(CO_2)} = 3.3 \times 10^{-7} \left[\text{mol L}^{-1} \text{ Pa}^{-1}\right] \quad (30)$$

$$K^\circ_{H(NH_3)} = 6.0 \times 10^{-4} \left[\text{mol L}^{-1} \text{ Pa}^{-1}\right] \quad (31)$$

$$K^\circ_X = 7 \times 10^{0} \left[\text{mol}^{-1} \text{ L}\right] \quad (32)$$

$$K^\circ_Y = 1.7 \times 10^{7} \left[\text{mol}^{-1}\text{L}\right] \quad (33)$$

$$K_b^\circ = 1.8 \times 10^{-5}\ [\mathrm{mol\ L^{-1}}] \quad (34)$$

$$(\text{or } pK_a^\circ = 9.3) \quad (35)$$

$$K_1^\circ = 4.4 \times 10^{7}\ [\mathrm{mol^{-1}\ L}] \quad (36)$$

$$K_2^\circ = 4.6 \times 10^{3}\ [\mathrm{mol^{-1}\ L}] \quad (37)$$

$$K_W^\circ = 1.0 \times 10^{-14}\ [\mathrm{mol^2\ L^{-2}}] \quad (38)$$

Note that the superscript (°) represents the values for aqueous ammonia at 25 °C in the limit of zero ionic strength. In addition to the above mass action laws, conservation laws apply as well. Specifically, charge neutrality must be preserved globally and locally. Charge neutrality can be described as follows:

$$[A_{eff}] + [H^+] = [HCO_3^-] + 2[CO_3^{2-}] + [OH^-] \quad (39)$$

where,

$$[A_{eff}] \equiv [NH_4^+] - [NH_2COO^-] + [A_{res}] \quad (40)$$

Note that $[A_{eff}]$ represents the effective alkalinity. In contrast to strong-base alkaline solutions such as potassium hydroxide solutions, alkalinity in aqueous ammonia is not constant but a function of pH which is set by the equilibria defined using eqn (16), (17) and (20). $[A_{res}]$ denotes the contributions originating from other charged species that do not appear in the chemical reactions but can be part of the solution, *e.g.*, Na^+, Cl^- or Br^-. $[A_{res}]$ is defined as the sum of all the residual positive ions weighted by their charge minus the sum of all the residual negative charges weighted by their charge.

We define the molar density of the total nitrogen as [N], which is constant. According to mass conservation,

$$[N] = [RNHCOOH] + [RNHCOO^-] + [NH_3] + [NH_4^+] \quad (41)$$

Substituting eqn (23)–(25) into eqn (41) yields:

$$[NH_4^+] = \frac{K_b[N]}{K_b + [OH^-] + [OH^-]K_X[CO_2] + K_XK_Y[CO_2][OH^-]^2} \quad (42)$$

Substituting eqn (23), (24), (26), (27) and (42) into eqn (39) yields an essential equation of this system:

$$[A_{res}] + \frac{[N]\left(K_b - K_XK_Y[CO_2][OH^-]^2\right)}{K_b + [OH^-] + [CO_2]\left(K_X[OH^-] + K_XK_Y[OH^-]^2\right)} = [CO_2]\left(K_1[OH^-] + 2K_1K_2[OH^-]^2\right) + [OH^-] \quad (43)$$

Eqn (43) is a quadratic equation for $[CO_2]$ and thus $[CO_2]$ can be explicitly expressed as function of only one variable, $[OH^-]$:

$$[CO_2] = f([OH^-]) \equiv \frac{\beta}{2\alpha}\left(\sqrt{1 - \frac{4\alpha\gamma}{\beta^2}} - 1\right) \quad (44)$$

where,

$$\alpha = [OH^-]^4 2K_XK_YK_1K_2 + [OH^-]^3K_XK_1(K_Y + 2K_2) + [OH^-]^2K_XK_1 \quad (45)$$

$$\beta = [OH^-]^3(2K_1K_2 + K_XK_Y) + [OH^-]^2(K_1 + 2K_bK_1K_2 + K_X + K_XK_Y([N] - [A_{res}]) + [OH^-](K_bK_1 - K_X[A_{res}])) \quad (46)$$

$$\gamma = [OH^-]^2 + [OH^-](K_b - [A_{res}]) - K_b([N] + [A_{res}]) \quad (47)$$

The other root of eqn (43) always takes a negative value and thus is not physical. In this section, we assume $[A_{res}] \sim 0$ for simplification. In this case, β and γ simplify to:

$$\beta = [OH^-]^3(2K_1K_2 + K_XK_Y) + [OH^-]^2(K_1 + 2K_bK_1K_2 + K_X + K_XK_Y[N]) + [OH^-]K_bK_1 \quad (48)$$

$$\gamma = [OH^-]^2 + K_b[OH^-] - K_b[N] \quad (49)$$

Eqn (45), (48) and (49) indicate that γ can mathematically take negative values while α and β are guaranteed to be positive. However, substituting $\gamma > 0$ into eqn (44) yields $[CO_2] < 0$. Therefore, there is a physical upper bound for $[OH^-]$ (*i.e.*, $[OH^-]_{max}$) so that γ is kept negative or zero, which is discussed later in more detail. $\frac{\beta}{2\alpha}\sqrt{1 - \frac{4\alpha\gamma}{\beta^2}} - 1$, γ and $[CO_2]$ are plotted in Fig. 1, 2, 3 and 4, respectively. These figures confirm the mathematical and physical limits summarized in Table 1.

Conversely, $[OH^-]$ can be implicitly expressed as a function of only one variable, $[CO_2]$:

$$[OH^-] = f^{-1}([CO_2]) \quad (50)$$

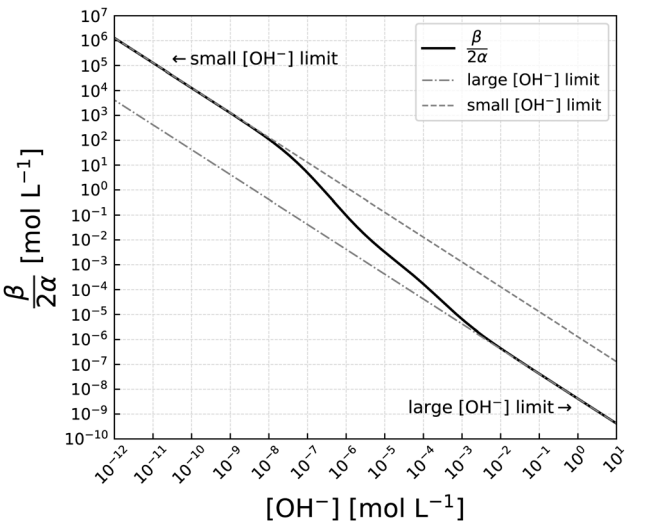

Fig. 1 $\frac{\beta}{2\alpha}$ as a function of $[OH^-]$ for [N] = 2 mol L^{-1} and T = 25 °C.

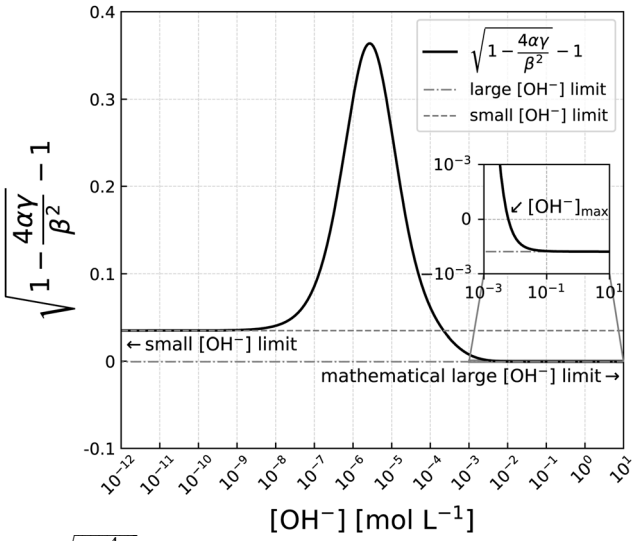

Fig. 2 $\sqrt{1-\frac{4\alpha\gamma}{\beta^2}}-1$ as a function of [OH$^-$] for [N] = 2 mol L^{-1} and T = 25 °C. Note that $\sqrt{1-\frac{4\alpha\gamma}{\beta^2}}-1$ takes negative values at [OH$^-$] > [OH$^-$]$_{max}$.

By substituting eqn (50) into eqn (42), [NH_4^+] can be implicitly expressed as a function of only one variable, [CO_2], as:

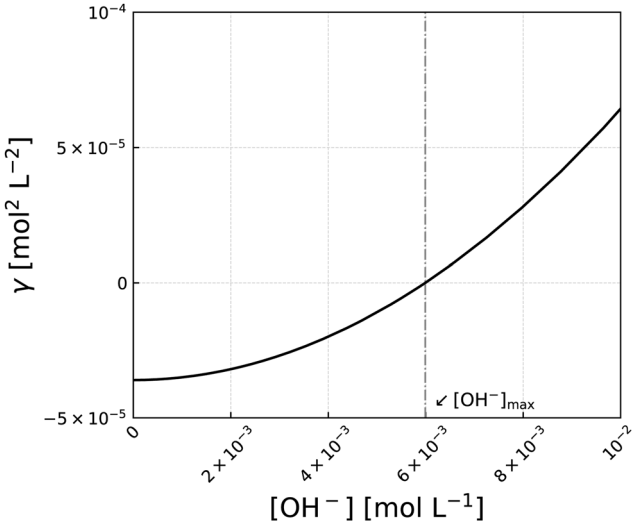

Fig. 3 γ as a function of [OH$^-$] for [N] = 2 mol L^{-1} and T = 25 °C.

$$[NH_4^+] = \frac{K_b[N]}{K_b + f^{-1}([CO_2])\{1 + K_X[CO_2](1 + f^{-1}([CO_2])K_Y)\}} \quad (51)$$

$$\equiv g([CO_2]) \quad (52)$$

Therefore, the effective alkalinity [A_{eff}] can be expressed as:

$$[A_{eff}] = g([CO_2]) \times \left(1 - \frac{K_X K_Y}{K_b}[CO_2]\{f^{-1}([CO_2])\}^2\right) \quad (53)$$

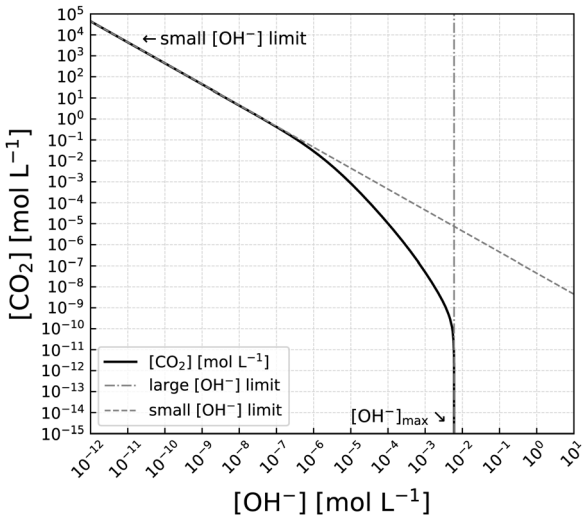

Fig. 4 [CO_2] as a function of [OH$^-$] for [N] = 2 mol L^{-1} and T = 25 °C.

Fig. 5–7 show plots of the effective alkalinity and concentration of each chemical species, assuming [N] = 2 mol L^{-1} and T = 25 °C.

The CO_2 loading status θ can be defined as:

$$\theta \equiv \theta_{DOC} + \theta_{DIC} \quad (54)$$

where,

$$\theta_{DOC} \equiv \frac{[DOC]}{[N]} \quad (55)$$

$$\theta_{DIC} \equiv \frac{[DIC]}{[N]} \quad (56)$$

Note that DOC and DIC represent dissolved organic carbon and dissolved inorganic carbon, respectively, which are defined as:

$$[DOC] \equiv [NH_2COOH] + [NH_2COO^-] \quad (57)$$

$$[DIC] \equiv [CO_2] + [HCO_3^-] + [CO_3^{2-}] \quad (58)$$

Therefore,

$$\theta = \frac{K_X}{K_b[N]} g([CO_2])[CO_2] f^{-1}([CO_2])\left(1 + K_Y f^{-1}([CO_2])\right) + \frac{[CO_2]}{[N]}\left(1 + K_1 f^{-1}([CO_2]) + K_1 K_2 \{f^{-1}([CO_2])\}^2\right) \quad (59)$$

This equation can be numerically plotted against P_{CO_2} or pH, as is shown in Fig. 8 and 9, assuming [N] = 2 mol L^{-1} and T = 25 °C.

3.1.1 Large [OH$^-$] limit. Eqn (44) indicates that [CO_2] becomes zero when γ = 0. In this case, [OH$^-$]$_{max}$ satisfies the following equation:

$$[OH^-]_{max}^2 + K_b[OH^-]_{max} - K_b[N] = 0 \quad (60)$$

Table 1 Summary of small or large $[OH^-]$ limits. δ_1 and δ_2 in this table are positive numbers defined as $\delta_1 \equiv \sqrt{1+\frac{4K_X[N]}{K_bK_1}}-1$ and $\delta_2 \equiv -\frac{2K_1K_2+K_XK_Y}{4K_XK_YK_1K_2}\left(\sqrt{1-\frac{8K_XK_YK_1K_2}{(2K_1K_2+K_XK_Y)^2}}-1\right)$, respectively. DICI stands for dissolved inorganic carbon as ions, namely, CO_3^{2-} and HCO_3^-

Parameter or variable	Limit of a small $[OH^-]$	Physical limit of a large $[OH^-]$	Unphysical limit of a large $[OH^-]$
$[OH^-]$	$[OH^-] \to 0$	$[OH^-] \to [OH^-]_{max}$	$[OH^-] \to \infty$
$\frac{\beta}{2\alpha}$	$\frac{K_b}{2K_X[OH^-]} \to \infty$	$\frac{2K_1K_2+K_XK_Y}{4[OH^-]_{max}K_XK_YK_1K_2} \to$ finite	$\frac{2K_1K_2+K_XK_Y}{4[OH^-]K_XK_YK_1K_2} \to +0$
$\sqrt{1-\frac{4\alpha\gamma}{\beta^2}}-1$	$\delta_1 \to$ finite	0	$\sqrt{1-\frac{8K_XK_YK_1K_2}{(2K_1K_2+K_XK_Y)^2}}-1<0$
$[CO_2]$	$\frac{K_b}{2K_X[OH^-]}\delta_1 \to \infty$	0	$-\frac{\delta_2}{[OH^-]}<0$
$[A_{eff}]$	$\frac{K_bK_1}{2K_X}\delta_1 \to$ finite	$[OH^-]_{max} \to$ finite	$\frac{K_XK_Y[N]\delta_2}{1-K_XK_Y\delta_2} \to$ finite
$[NH_4^+]$	$\frac{K_bK_1}{2K_X}\delta_1 \to$ finite	$[OH^-]_{max} \to$ finite	$\frac{K_b[N]}{[OH^-](1-K_XK_Y\delta_2)} \to 0$
$[NH_2COOH]$	$\frac{K_bK_1}{4K_X}\delta_1^2 \to$ finite	0	$-\frac{K_X[N]\delta_2}{[OH^-](1-K_XK_Y\delta_2)} \to 0$
$[NH_2COO^-]$	$\frac{K_bK_1K_Y[OH^-]}{4K_X}\delta_1^2 \to 0$	0	$-\frac{K_XK_Y[N]\delta_2}{1-K_XK_Y\delta_2} \to$ finite
$[NH_3]$	$\frac{K_1[OH^-]}{2K_X}\delta_1 \to 0$	$\frac{[OH^-]_{max}^2}{K_b} \to$ finite	$\frac{[N]}{1-K_XK_Y\delta_2} \to$ finite
$[HCO_3^-]$	$\frac{K_bK_1}{2K_X}\delta_1 \to$ finite	0	$-K_1\delta_2 < 0$
$[CO_3^{2-}]$	$\frac{K_bK_1K_2[OH^-]}{2K_X}\delta_1 \to 0$	0	$-K_1K_2[OH^-]\delta_2 \to -\infty < 0$
θ_{DOC}	$\frac{K_bK_1}{4K_X[N]}\delta_1^2 \to$ finite	0	$-\frac{K_XK_Y\delta_2}{1-K_XK_Y\delta_2} \to$ finite
θ_{DICI}	$\frac{K_bK_1}{2K_X[N]}\delta_1 \to$ finite	0	$-\frac{K_1K_2[OH^-]\delta_2}{[N]} \to -\infty < 0$
$\theta_{DOC}+\theta_{DICI}$	1	0	$-\frac{K_1K_2[OH^-]\delta_2}{[N]} \to -\infty < 0$
θ	$1+\frac{[CO_2]}{[N]} \to 1+\infty$	0	$-\frac{K_1K_2[OH^-]\delta_2}{[N]} \to -\infty < 0$

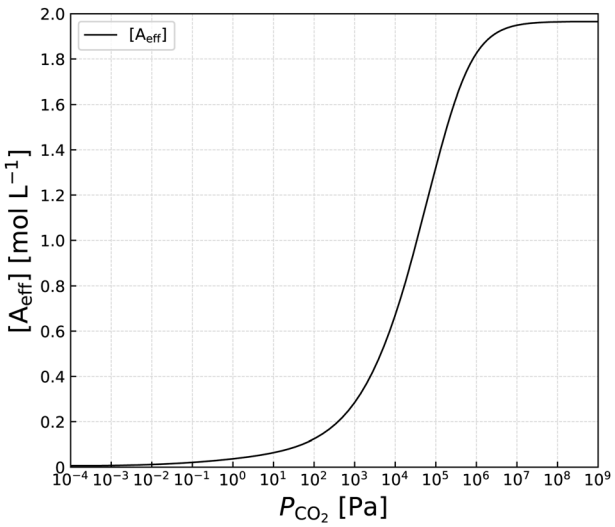

Fig. 5 The effective alkalinity $[A_{eff}]$ as a function of P_{CO_2} for [N] = 2 mol L^{-1} and T = 25 °C.

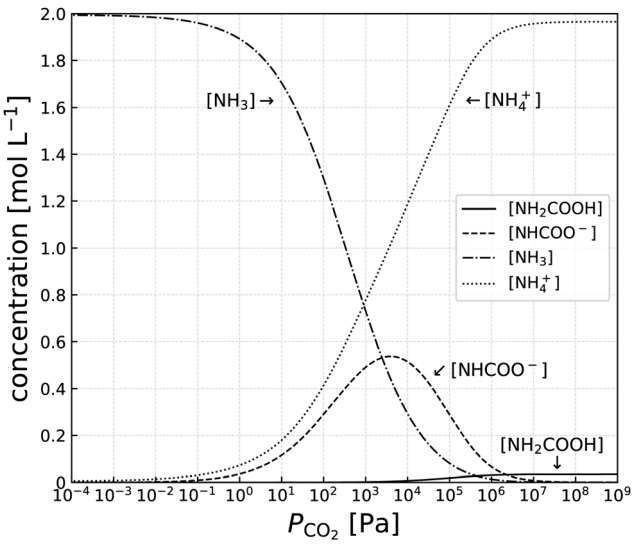

Fig. 6 Concentrations of DOC components as a function of P_{CO_2} for [N] = 2 mol L^{-1} and T = 25 °C.

or,

$$[OH^-]_{max} = \frac{K_b}{2}\left(\sqrt{1+\frac{4[N]}{K_b}}-1\right) \quad (61)$$

If $[OH^-]$ exceeds $[OH^-]_{max}$, it results in $[CO_2] < 0$. Since $[CO_2]$ needs to be positive, $[OH^-]_{max}$ set the maximum pH of this

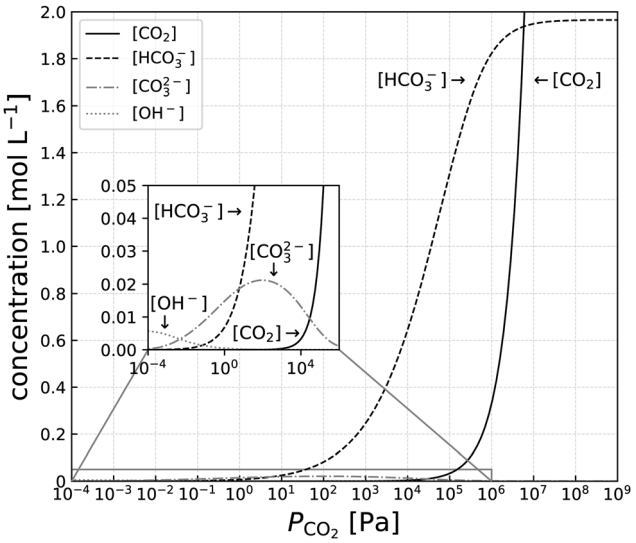

Fig. 7 Concentrations of DIC components and [OH$^-$] as a function of P_{CO_2} for [N] = 2 mol L^{-1} and T = 25 °C.

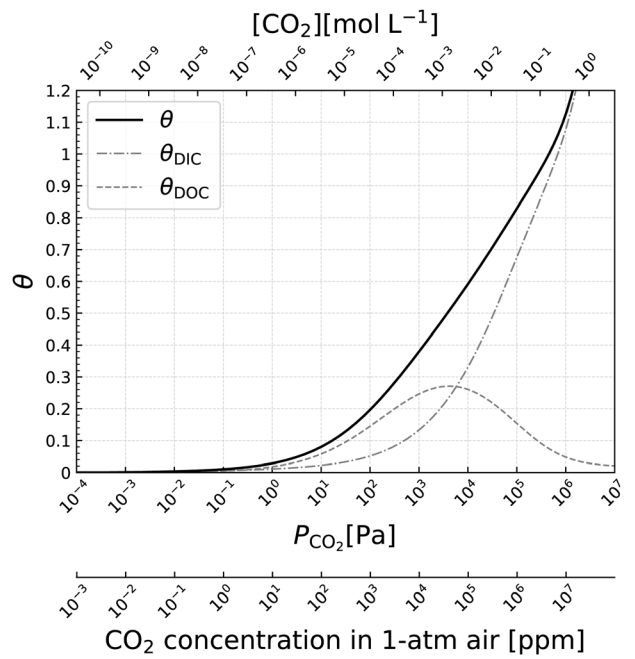

Fig. 8 θ and each component (θ_{DIC} and θ_{DOC}) as a function of P_{CO_2}, [CO_2] or CO_2 concentration in 1 atm air for [N] = 2 mol L^{-1} and T = 25 °C.

system. Substituting [N] = 2 mol L^{-1} and eqn (34) into eqn (61) yields:

$$[OH^-]_{max} = 5.99 \times 10^{-3}\ [\text{mol L}^{-1}] \quad (62)$$

or,

$$pH_{max} = pH(\theta = 0) = 11.77 \quad (63)$$

This value is in agreement with the pH of a 2 mol L^{-1} pure aqueous ammonia which does not include any DIC or DOC.

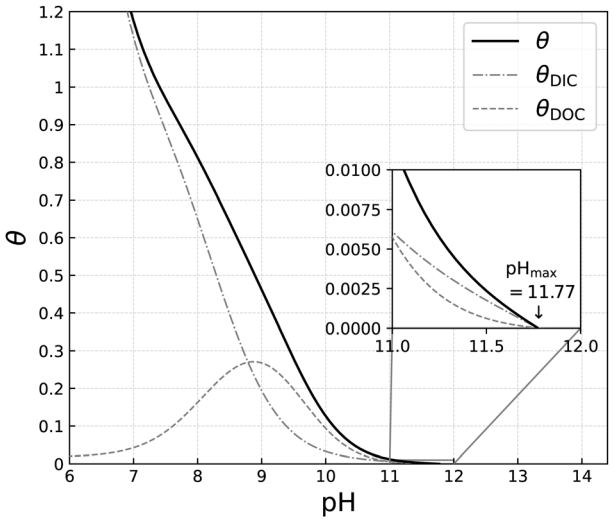

Fig. 9 θ and each component (θ_{DIC} and θ_{DOC}) as a function of pH for [N] = 2 mol L^{-1} and T = 25 °C.

Although this is the physical maximum limit of [OH$^-$] corresponding to [CO_2] = 0, one can mathematically take the limit of [OH$^-$] $\rightarrow \infty$. Although this is an unphysical case because this mathematical limit results in negative values of [CO_2], investigating this asymptotical behavior is useful to understand the global structure of the governing equation of this system, *i.e.*, eqn (44). Both unphysical limits (in other words, mathematical limits) and physical limits have been derived and summarized in Table 1.

It is also notable that [A_{res}] affects the value of [OH$^-$]$_{max}$ if [A_{res}] $\neq$ 0. In this case, [OH$^-$]$_{max}$ can be expressed as:

$$[OH^-]_{max} = \frac{K_b - [A_{res}]}{2}\left(\sqrt{1 + \frac{4K_b([N] + [A_{res}])}{(K_b - [A_{res}])^2}} - 1\right) \quad (64)$$

3.1.2 Small [OH$^-$] limit. Fig. 5, 6 and 8 suggest that [A_{eff}], [NH_4^+], [NH_2COOH] and θ_{DOC} converge to constant values as [CO_2] $\rightarrow \infty$ (in other words, as [OH$^-$] $\rightarrow$ 0), respectively. The analytical expressions for these limits have been derived and summarized in Table 1. For details, see the ESI.†

3.1.3 Large K_b limit. When $K_b \gg$ [OH$^-$] is satisfied, eqn (42) results in:

$$[NH_4^+] \sim [N] \quad (65)$$

Therefore,

$$[RNH_2] \sim 0 \quad (66)$$

$$[RNHCOOH] \sim 0 \quad (67)$$

$$[RNHCOO^-] \sim 0 \quad (68)$$

In this limit, the model simplifies to the isotherm model of alkaline aqueous solutions in a hydroxide–carbonate–bicarbonate system with a constant alkalinity of [N], which is identical to the model derived in the previous paper.[20]

3.2 Generalization to aqueous amine solutions

In aqueous amine solutions, the equilibrium coefficients K_X, K_Y and K_b can differ from those in aqueous ammonia and will depend on specific materials used as a sorbent. Therefore, we rename these equilibrium coefficients depending on a specific amine as K_{XR}, K_{YR} and K_{bR}, respectively. In the case of primary amines, the chemical reactions can be described as:

$$H_2O_{(g)} \overset{K_{H(H_2O)}}{\rightleftharpoons} H_2O_{(aq)} \quad (69)$$

$$CO_{2(g)} \overset{K_{H(CO_2)}}{\rightleftharpoons} CO_{2(aq)} \quad (70)$$

$$RNH_2 + CO_{2(aq)} \overset{K_{XR}}{\rightleftharpoons} RNHCOOH \quad (71)$$

$$RNHCOOH + OH^- \overset{K_{YR}}{\rightleftharpoons} H_2O + RNHCOO^- \quad (72)$$

$$RNH_2 + H_2O \overset{K_{bR}}{\rightleftharpoons} RNH_3^+ + OH^- \quad (73)$$

$$CO_{2(aq)} + OH^- \overset{K_1}{\rightleftharpoons} HCO_3^- \quad (74)$$

$$HCO_3^- + OH^- \overset{K_2}{\rightleftharpoons} CO_3^{2-} + H_2O \quad (75)$$

where, K_{XR}, K_{YR} and K_{bR} are defined as:

$$K_{XR} \equiv \frac{[RNHCOOH]}{[NH_3][CO_2]} \quad (76)$$

$$K_{YR} \equiv \frac{[RNHCOO^-]}{[RNHCOOH][OH^-]} \quad (77)$$

$$K_{bR} \equiv \frac{[RNH_3^+][OH^-]}{[RNH_2]} \quad (78)$$

In the case of secondary amines, we need to replace RH with RR′. Therefore, essentially the same key equation (eqn (44)) applies to aqueous primary and secondary amine solutions just by replacing K_X, K_Y and K_b with K_{XR}, K_{YR} and K_{bR}, respectively.

For tertiary amines, eqn (71) and eqn (72) do not apply. Therefore, we can obtain the model for tertiary amines by substituting $K_{XR} = 0$ and $K_{YR} = 0$. The resulting key equation for tertiary amines corresponding to eqn (44) for primary and secondary amines can be expressed as:

$$[CO_2] = \frac{-[OH^-]^2 + [OH^-]([A_{res}] - K_{bR}) + K_{bR}([A_{res}] + [N])}{K_1[OH^-](1 + 2K_2[OH^-])(K_{bR} + [OH^-])} \quad (79)$$

3.3 Generalization to amine solids

The main difference between aqueous amine solutions and amine solids is that water concentration in amine solids is not large enough to be regarded as constant. Also, hydration water around ions need to be taken into consideration, as follows:

$$CO_{2(g)} \overset{K_{H(CO_2)R}}{\rightleftharpoons} CO_{2(aq)} \quad (80)$$

$$RNH_2 + CO_{2(aq)} \overset{K_{XR}}{\rightleftharpoons} RNHCOOH \quad (81)$$

$$RNHCOOH + OH^-(H_2O)_z \overset{K_{YR(eff)}}{\rightleftharpoons} n_3H_2O + RNHCOO^-(H_2O)_p \quad (82)$$

$$RNH_2 + n_4H_2O \overset{K_{bR(eff)}}{\rightleftharpoons} RNH_3^+(H_2O)_q + OH^-(H_2O)_z \quad (83)$$

$$CO_{2(aq)} + OH^-(H_2O)_z \overset{K_{1R(eff)}}{\rightleftharpoons} HCO_3^-(H_2O)_x + n_1H_2O \quad (84)$$

$$HCO_3^-(H_2O)_x + OH^-(H_2O)_z + n_2H_2O \overset{K_{2R(eff)}}{\rightleftharpoons} CO_3^{2-}(H_2O)_y \quad (85)$$

p, q, x, y and z represent the hydration numbers of $RNHCOO^-$, RNH_3^+, HCO_3^-, CO_3^{2-} and OH^-, respectively. The stoichiometric coefficients n_1, n_2, n_3 and n_4 can be expressed as:

$$n_1 = -x + z \quad (86)$$

$$n_2 = -x + y - z - 1 \quad (87)$$

$$n_3 = -p + z - 1 \quad (88)$$

$$n_4 = q + z + 1 \quad (89)$$

The equilibrium coefficients and Henry's constant are defined as:

$$K_{H(CO_2)R} \equiv \frac{[CO_2]}{P_{CO_2}} \quad (90)$$

$$K_{XR} \equiv \frac{[RNHCOOH]}{[NH_3][CO_2]} \quad (91)$$

$$K_{YR} \equiv \frac{\left[RNHCOO^-(H_2O)_p\right][H_2O]^{n_3}}{[RNHCOOH]\left[OH^-(H_2O)_z\right]} \quad (92)$$

$$K_{bR} \equiv \frac{\left[RNH_3^+(H_2O)_q\right]\left[OH^-(H_2O)_z\right]}{[RNH_2][H_2O]^{n_4}} \quad (93)$$

$$K_{1R} \equiv \frac{\left[HCO_3^-(H_2O)_x\right][H_2O]^{n_1}}{[CO_2]\left[OH^-(H_2O)_z\right]} \quad (94)$$

$$K_{2R} \equiv \frac{\left[CO_3^{2-}(H_2O)_y\right]}{\left[HCO_3^-(H_2O)_x\right]\left[OH^-(H_2O)_z\right][H_2O]^{n_2}} \quad (95)$$

Therefore, the same functional forms for aqueous amine solutions apply to solid amines by replacing K_{YR}, K_{bR}, K_1 and K_2 with $K_{YR(eff)}(\equiv K_{YR}[H_2O]^{-n_3})$, $K_{bR(eff)}(\equiv K_{bR}[H_2O]^{n_4})$, $K_{1R(eff)}$ $(\equiv K_{1R}[H_2O]^{-n_1})$ and $K_{2R(eff)}(\equiv K_{2R}[H_2O]^{n_2})$, respectively. In the same way for moisture-controlled CO_2 sorption in quaternary ammonium discussed in the previous paper,[20] the stoichiometric coefficients, n_1, n_2, n_3 and n_4 determine whether CO_2 affinity is enhanced or hindered due to the changes in the concentration of water inside the sorbent.

4 Result: validation of the framework of the model using the literature data of aqueous ammonia

In the previous section, we generalized the isotherm model of aqueous ammonia to amines, which is represented by the key equation, eqn (44). In this section, we calculate the CO_2 isotherms of aqueous ammonia and partial pressure of gaseous ammonia by substituting the specific values of the equilibrium coefficients from the literature into this key equation. The resulting CO_2 isotherms and P_{NH_3} of aqueous ammonia are compared to the experimental isotherm data from Pexton and Badger (1938).[33] Since this experimental data set was not obtained at 25 °C which is typically used as a modern standard, we calculated our model at 20 °C and 40 °C so that we could compare the model to the experimental data. Note that the isotherm data reported by Pexton and Badger (1938) has also been used in other research studies[34–36] to compare to the two thermodynamic models for electrolyte solutions: the extended universal quasichemical (UNIQUAC) model[36,37] and the electrolyte non random two liquid (e-NRTL) model.[38,39]

The values of K_H, K_1, K_2 and K_W for the temperature ranging from 0 °C to 40 °C are given as a function of temperature T in the literature.[26–28] Substituting T = 20 °C or T = 40 °C into these equations yields:

$$K_{H(CO_2)}(T = 20\ ^\circ\mathrm{C}) = 3.8 \times 10^{-7}\ [\mathrm{mol\ L^{-1}\ Pa^{-1}}] \quad (96)$$

$$K_1(T = 20\ ^\circ\mathrm{C}) = 6.1 \times 10^{7}\ [\mathrm{mol^{-1}\ L}] \quad (97)$$

$$K_2(T = 20\ ^\circ\mathrm{C}) = 6.1 \times 10^{3}\ [\mathrm{mol^{-1}\ L}] \quad (98)$$

$$K_W(T = 20\ ^\circ\mathrm{C}) = 6.8 \times 10^{-15}\ [\mathrm{mol^{2}\ L^{-2}}] \quad (99)$$

$$K_{H(CO_2)}(T = 40\ ^\circ\mathrm{C}) = 2.3 \times 10^{-7}\ [\mathrm{mol\ L^{-1}\ Pa^{-1}}] \quad (100)$$

$$K_1(T = 40\ ^\circ\mathrm{C}) = 1.7 \times 10^{7}\ [\mathrm{mol^{-1}\ L}] \quad (101)$$

$$K_2(T = 40\ ^\circ\mathrm{C}) = 2.1 \times 10^{3}\ [\mathrm{mol^{-1}\ L}] \quad (102)$$

$$K_W(T = 40\ ^\circ\mathrm{C}) = 2.9 \times 10^{-14}\ [\mathrm{mol^{2}\ L^{-2}}] \quad (103)$$

As for K_X and K_Y, the values at T = 15, 25, 35 and 45 °C were summarized by Wang *et al.* (2011).[31] Interpolation of these values gives the values at T = 20 °C or T = 40 °C as:

$$K_X(T = 20\ ^\circ\mathrm{C}) = 6.9 \times 10^{0}\ [\mathrm{mol^{-1}\ L}] \quad (104)$$

$$K_Y(T = 20\ ^\circ\mathrm{C}) = 2.6 \times 10^{7}\ [\mathrm{mol^{-1}\ L}] \quad (105)$$

$$K_X(T = 40\ ^\circ\mathrm{C}) = 4.7 \times 10^{0}\ [\mathrm{mol^{-1}\ L}] \quad (106)$$

$$K_Y(T = 40\ ^\circ\mathrm{C}) = 5.3 \times 10^{6}\ [\mathrm{mol^{-1}\ L}] \quad (107)$$

Values of $K_{H(NH_3)}$ and K_b can be obtained from the study by Clegg and Brimblecombe (1989)[32] as:

$$K_{H(NH_3)}(T = 20\ ^\circ\mathrm{C}) = 7.6 \times 10^{-4}\ [\mathrm{mol\ L^{-1}\ Pa^{-1}}] \quad (108)$$

$$K_b(T = 20\ ^\circ\mathrm{C}) = 1.7 \times 10^{-5}\ [\mathrm{mol\ L^{-1}\ Pa^{-1}}] \quad (109)$$

$$K_{H(NH_3)}(T = 40\ ^\circ\mathrm{C}) = 3.0 \times 10^{-4}\ [\mathrm{mol\ L^{-1}\ Pa^{-1}}] \quad (110)$$

$$K_b(T = 40\ ^\circ\mathrm{C}) = 1.9 \times 10^{-5}\ [\mathrm{mol\ L^{-1}\ Pa^{-1}}] \quad (111)$$

Fig. 10 compares the model to the experimental data from Pexton and Badger (1938),[33] using these values. The temperature ranges from T = 20 °C to T = 40 °C, while the nitrogen density ranges from [N] = 0.128 mol L^{-1} to [N] = 2 mol L^{-1}. Pexton and Badger (1938) provided two independent data sets for each temperature and nitrogen density; one is θ against P_{CO_2} (figures in the left column of Fig. 10) and the other is P_{NH_3} against P_{CO_2} (figures in the right column of Fig. 10). These two data sets can be used to validate the model independently.

Fig. 10 shows that the overall shape of the model looks qualitatively consistent with the experimental data both at T = 20 °C and T = 40 °C; however, there is an obvious discrepancy in the absolute values. We observed that this discrepancy is minimal at [N] = 0.128 mol L^{-1} and grows as [N] increases. This trend clearly indicates the influence of ionic strength. Therefore, appropriate corrections need to be made to the values of the seven parameters (namely, $K_{H(CO_2)}$, $K_{H(NH_3)}$, K_b, K_1, K_2, K_X, and K_Y) in the model, according to the change in ionic strength. This is reasonable because the values we substituted into equilibrium coefficients and Henry's constants were those in which the influence of ionic strength was not taken into consideration.

Among the seven parameters, $K_{H(CO_2)}$, $K_{H(NH_3)}$ and K_X do not include ionic species in the corresponding reactions. In addition, K_1 and K_Y involve the ionic species that have the same charge on both sides of the corresponding reaction. Therefore, it is reasonable to assume that only K_b and K_2 are significantly affected by changes in ionic strength. However, aqueous ammonia contains only a tiny amount of carbonate ions (see Fig. 7) and indeed a quick parameter test confirms that the model is not very sensitive to the changes in K_2 values. Therefore, we identified K_b as the only parameter that needs to be tuned according to ionic strength.

Based on standard models of ionic strength, eqn (23) needs to be updated in terms of a thermodynamic equilibrium coefficient $K_{b(therm)}$:[40]

$$K_{b(therm)} \equiv \frac{a_{NH_4^+} a_{OH^-}}{a_{NH_3}} \quad (112)$$

$$= K_b \gamma_{NH_4^+} \gamma_{OH^-} \quad (113)$$

where, a_i and γ_i represent an activity and an activity coefficient of chemical species i, respectively. Note that K_b is the apparent equilibrium coefficient defined in eqn (25).

Therefore,

$$K_b = K_{b(therm)} \times {\gamma_\pm}^{-2} \quad (114)$$

where,

$$\gamma_\pm \equiv \sqrt{\gamma_{NH_4^+} \gamma_{OH^-}} \quad (115)$$

Eqn (114) suggests that we need to multiply ${\gamma_\pm}^{-2}$ with the original value of K_b. By fitting the model into the experimental data, we derived this multiplier for each [N] as ${\gamma_\pm}^{-2}$ = 1.8, 2.5, 3.1, 4.0, 4.8 for [N] = 0.128, 0.5, 1, 1.5, 2 mol L^{-1}, respectively (see Table 2). Fig. 11 shows the model in which these multipliers are applied. This plot demonstrates an excellent

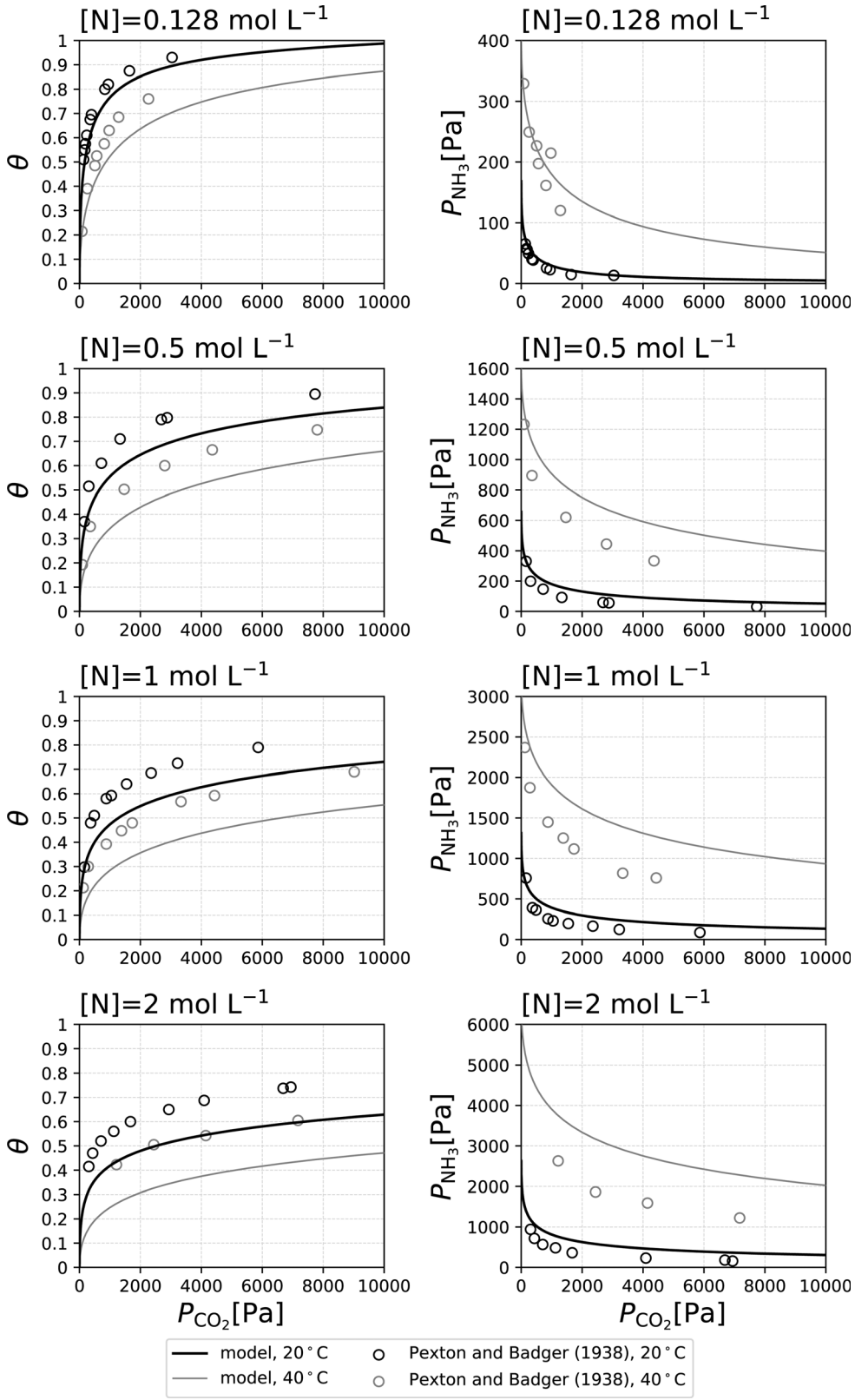

Fig. 10 A comparison between the experimental data reported by Pexton and Badger (1938) and the model at T = 20 °C or T = 40 °C before influence of ionic strength is corrected. Even though all the data have been used in the fitting procedure, some data points fall outside of the range of the graphs, and are only shown in the ESI.†

Table 2 Summary of the derived values of $\gamma_{\pm}^{-2}$ (= multiplier to K_b) and I. I is represented by the value at $P_{CO_2} \sim 2000$ Pa

[N] [mol L^{-1}]	T [°C]	$\gamma_{\pm}^{-2}$ (=multiplier to K_b)	I [mol L^{-1}]
0.128	20	1.8	0.118
0.128	40	Same as above	0.0960
0.5	20	2.5	0.399
0.5	40	Same as above	0.298
1	20	3.1	0.723
1	40	Same as above	0.534
1.5	20	4.0	1.04
1.5	40	No data points	0.782
2	20	4.8	1.36
2	40	Same as above	1.03

agreement between the model and the experimental data both at $T = 20^\circ$ and $T = 40^\circ$.

Fig. 13 shows $\gamma_{\pm}$ values that were calculated from these multipliers as a function of [N]. To make sure that these values of $\gamma_{\pm}$ are consistent with the Debye–Hückel theory,[40] next, we plotted $\gamma_{\pm}$ against ionic strength, I, which is defined as:

$$I = \frac{1}{2}\sum_i z_i^2 C_i \quad (116)$$

where, C_i and z_i represent the concentration and electrochemical valence (negative for anions) of each chemical species i, respectively. Although [N] is an indicator of I that monotonously increases as I increases, ionic strength is not only a function of [N] but also a function of P_{CO_2}, as is shown in Fig. 12. For simplification, we assume that I is virtually constant around the area from where the experimental data were collected (*e.g.*, at $P_{CO_2} \sim 2000$ Pa), which is indeed a very good approximation especially in the case of smaller [N] (see Fig. 12). Table 2 summarizes the ionic strength at $P_{CO_2} \sim 2000$ Pa. We take an average of the I values at different temperature and regard these values as approximately constant values for each nitrogen density, *i.e.*, I = 0.107, 0.349, 0.628, 0.913 and 1.19 mol L^{-1} for [N] = 0.128, 0.5, 1, 1.5 and 2 mol L^{-1}, respectively. These values confirm a linear relation between I and [N]. In Fig. 14, the $\gamma_{\pm}$ values obtained from the fitting are compared to those obtained from the Debye–Hückel theory.[40] The Debye–Hückel limiting law, which is valid for very dilute solutions corresponding to ionic strength $< 1 \times 10^{-3}$ mol L^{-1}, is expressed as:[40]

$$\log_{10}\gamma_{\pm} = -A|z_+ z_-|\sqrt{I} \quad (117)$$

where A = 0.510 mol$^{-1/2}$ L$^{1/2}$ for water at 25 °C.[40] In our case, $z_+ = 1$ and $z_- = -1$. For moderate concentrations corresponding to the ionic strength ranging from 1×10^{-3} mol L^{-1} to 0.1 mol L^{-1}, the following Debye–Hückel equation[40] applies:

$$\log_{10}\gamma_{\pm} = -A|z_+ z_-|\frac{\sqrt{I}}{1+\sqrt{I}} \quad (118)$$

Fig. 14 confirms that the $\gamma_{\pm}$ obtained from the fitting between the model and experimental data shows a very good agreement with the Debye–Hückel equation at $I \lesssim 0.1$ mol L^{-1}. As ionic strength becomes larger than $\gtrsim$0.1 mol L^{-1}, the deviation from the Debye–Hückel equation increases, as is expected.

5 Discussion

We have demonstrated that the binary CO_2–H_2O isotherm reduced to a single key analytical equation, eqn (44), regardless of weak-base, strong-base, aqueous alkaline solutions, aqueous amine solutions or amine solids, which is far from trivial. It is especially notable that, even though this equation includes a square root and several high order terms both in the nominator and the denominator, Fig. 1 through Fig. 9 shows that the mathematical structure of this model has indeed very simple but characteristic and non-trivial features. For example, Fig. 2 indicates that the function $\sqrt{1-\frac{4\alpha\gamma}{\beta^2}}-1$ has a single maximum value and the functional shape is almost symmetrical around that point when it is plotted on a linear scale for the vertical axis and on a log scale for the horizontal axis, which is almost impossible to tell until one draws the plot. It is also important to compare this model to the experimental isotherm data as well as conduct further mathematical investigations on this model. The mathematical framework of the model has been validated using the experimental data from aqueous ammonia (a weak-base aqueous solution) in a quantitative way. Note that this model has already been validated for strong-base quaternary ammonium.[20] These experimental validations and the theoretical framework developed in this paper indicate that this general model most likely applies to solid amines in the same way; however, experimental validation using solid amines will be nencessary in order to strengthen this model furthermore.

It should be noted that the parameters one obtains for different combinations of amines are not independent. For example, the ionic strength effects should be the same for different compositions, affecting K_b of different amines in similar ways. The carbonate/bicarbonate chemistry may be affected by water activity, but is not dependent on the choice of amine. If different amines are present, their ability to form carbamates or accept protons should be the same in each environment. Therefore, this approach greatly reduces the degrees of freedom one needs to consider in the analysis of complex amine solutions or solids. For example, the moisture swing effect visible in strong-base AEMs should still be present in weak-base AEMs even if it is obscured by other interactions of water with the primary or secondary amine.

6 Conclusions

In this paper, first we have identified a single key analytical equation, eqn (44), which represents a model of CO_2 isotherms and NH_3 isotherms for aqueous ammonia, *i.e.*, a weak-base alkaline solution. It is notable that we can analytically calculate θ or P_{NH_3} from P_{CO_2} and nitrogen density [N] just based on this key equation without relying on complicated numerical solvers.

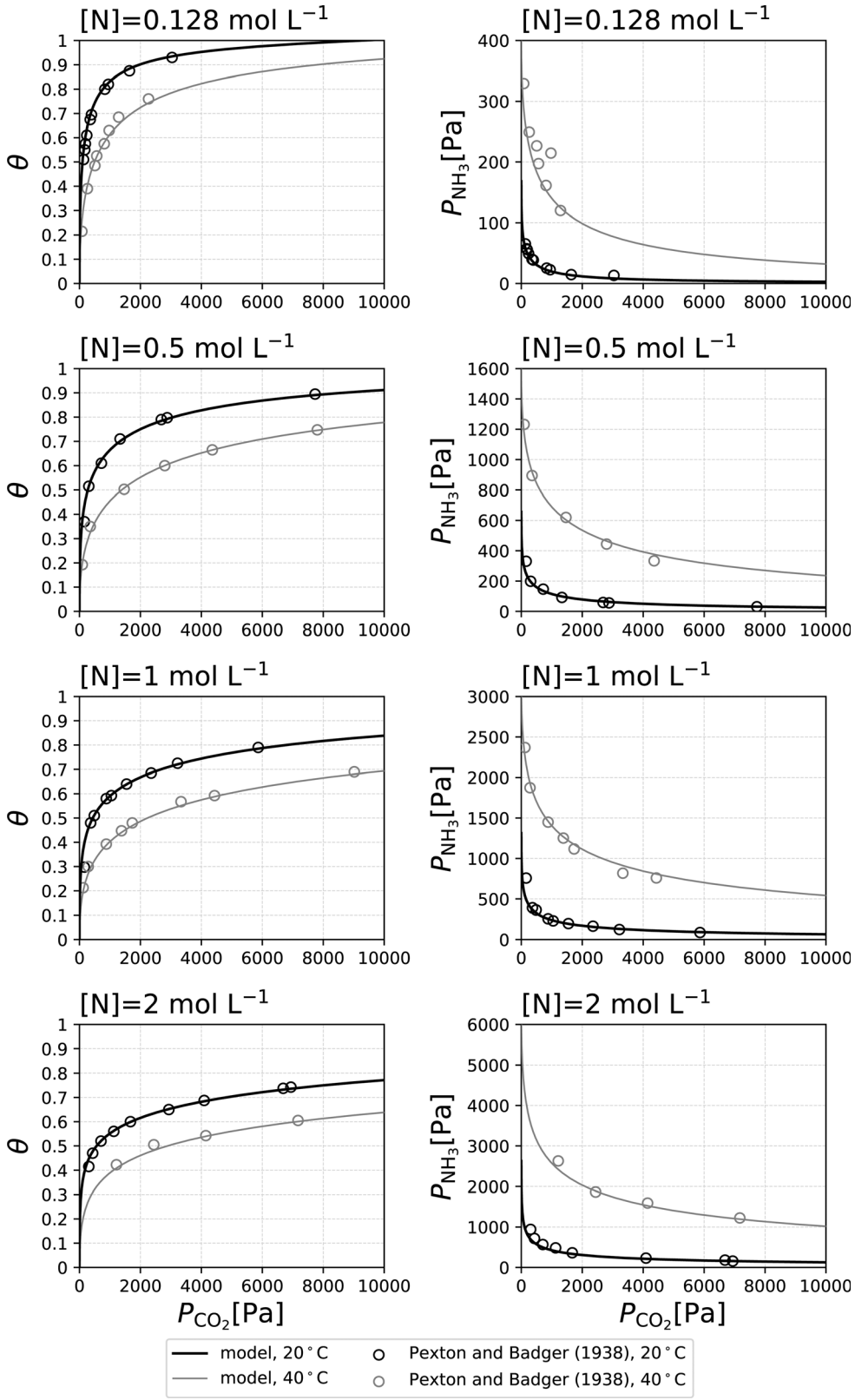

Fig. 11 A comparison of the experimental data reported by Pexton and Badger (1938) and the model at T = 20 °C or T = 40 °C after the $\gamma_{\pm}$ values summarized in Table 2 are applied to correct the influence of ionic strength. Even though all the data have been used in the fitting procedure, some data points fall outside of the range of the graphs. These points are also well fit, and are shown on a logarithmic scale in the ESI.†

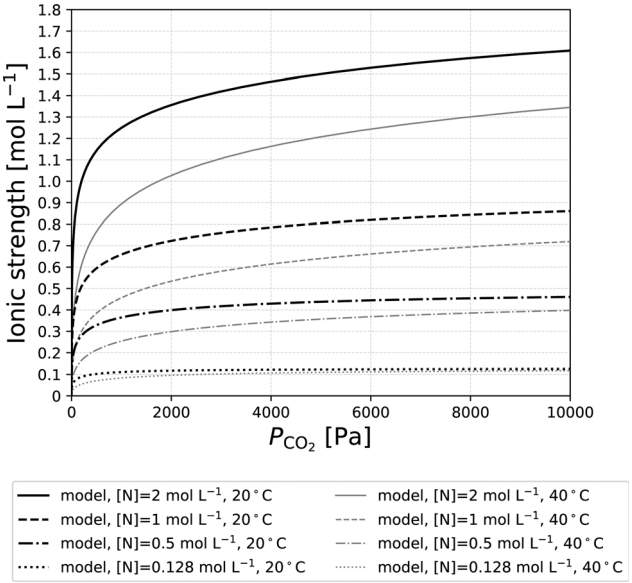

Fig. 12 Ionic strength calculated from the model at T = 20 °C and T = 40 °C and for [N] = 0.128, 0.5, 1, 1.5 and 2 mol L^{-1}. Note that the $\gamma_{\pm}$ values have already been applied.

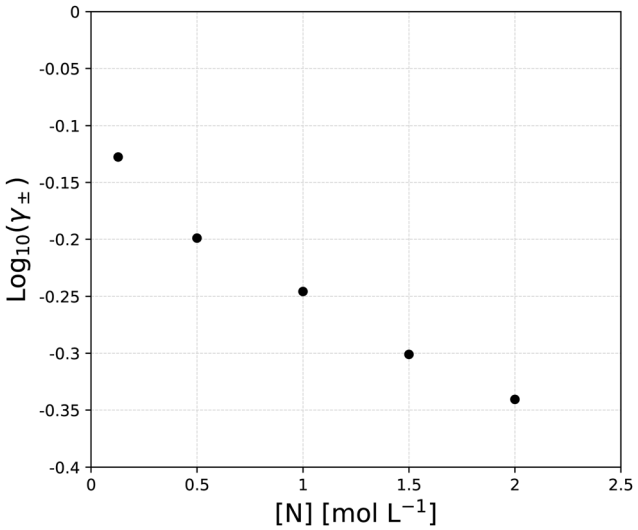

Fig. 13 $\gamma_{\pm}$ values obtained from the fitting between the model and the experimental data reported by Pexton and Badger (1938) for each [N].

Non-trivial mathematical features of eqn (44) are explicitly visualized in Fig. 1 through Fig. 9. Also, the asymptotic analysis has been conducted and the results have been summarized in Table 1, all of which are of theoretical interest.

The predictive capability of this analytic model for weak-base alkaline solutions has been validated using the experimental data of aqueous ammonia at different temperatures and nitrogen densities in the literature,[33] ranging from T = 20 °C to T = 40 °C and from [N] = 0.128 mol L^{-1} to [N] = 2 mol L^{-1}. Initially, we directly compared the model using apparent equilibrium coefficients to the experimental data (Fig. 10).

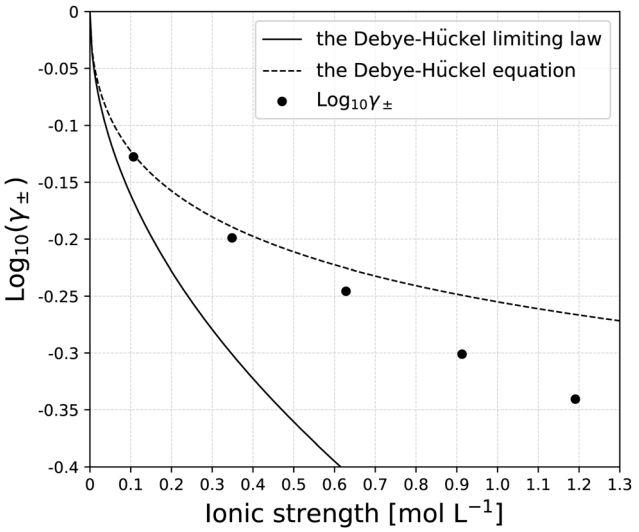

Fig. 14 A comparison between the Debye–Hückel theory and $\gamma_{\pm}$ values obtained from the fitting.

This comparison clarified that the influence of ionic strength needs to be taken into consideration, especially for the solutions of higher [N]. Based on theoretical reasoning and a quick parameter test, we identified that K_b is the only relevant parameter which is strongly affected by ionic strength. The activity coefficient $\gamma_{\pm}$ relevant to K_b has been calculated for [N] = 0.128, 0.5, 1, 1.5 and 2 mol L^{-1} by fitting the model to the experimental data (see Table 2). Indeed, these $\gamma_{\pm}$ values yielded an excellent match between the model and the experimental data (Fig. 11). The calculated values of $\gamma_{\pm}$ have been compared to the Debye–Hückel theory. As a result, we confirmed that $\gamma_{\pm}$ shows a very good agreement with the prediction from the Debye–Hückel equation at $I \lesssim 0.1$ mol L^{-1}, where the Debye–Hückel equation is supposed to be valid. As the ionic strength increases beyond $\lesssim$0.1 mol L^{-1}, the calculated $\gamma_{\pm}$ values start deviating from the Debye–Hückel equation, as was expected. Hence, we conclude that this model applies to aqueous ammonia in a very quantitative way.

This CO_2 isotherm model for weak-base alkaline solution represented by eqn (44) also applies to strong-base alkaline solutions just by taking a special limit of $K_b \gg [OH^-]$. In the previous paper, we generalized the CO_2 isotherm theory of strong-base alkaline solutions to that of strong-base anion exchange materials.[20] In the same way, here we generalized the CO_2 isotherm model for weak-base alkaline solution to amine solutions and finally to solid primary, secondary and tertiary amines in this paper. We can apply essentially the same model as used for weak-base alkaline solutions (eqn (44)) to amine solutions but the values of the three parameters, K_X, K_Y and K_b, need to be updated to K_{XR}, K_{YR} and K_{bR} because it is likely that these values differ between aqueous ammonia and amine solutions. Furthermore, for amine solids, the concentration of water is not large enough to be regarded as constant in the mass action laws unlike in aqueous solutions. Hence, we generalized the model to solid amines by updating K_{YR},K_{bR},K_1

and K_2 to $K_{YR(eff)}$,$K_{bR(eff)}$,$K_{1R(eff)}$ and $K_{2R(eff)}$, all of which effectively vary according to the water concentration terms in the corresponding mass action laws. Whether water enhances or hinders CO_2 sorption is determined by stoichiometric coefficients in the elementary chemical reactions by taking hydration water around the counterions in the sorbents into consideration.

This work shows that the moisture-swing model that had been established in quaternary ammonium[20] was a special case of the general binary CO_2–H_2O isotherm model for amines. The resulting general model is represented by a simple analytical equation, eqn (44), but can be applied to a very wide range of CO_2 sorbents including weak-base or strong-base aqueous alkaline solutions, aqueous amine solutions and solid amines with primary, secondary and tertiary amines. This model allows us to deal with the influence of water in a continuous way, eliminating the need to discuss anhydrous states and wet states separately. This analytic model will provide a firm basis for exploring applications of moisture-controlled CO_2 sorption in general amines beyond quaternary ammonium.

Author contributions

Yuta Kaneko: conceptualization, investigation, methodology, visualization, and writing (original draft). Klaus S. Lackner: conceptualization, supervision, validation, and writing (review and editing).

Conflicts of interest

Klaus S. Lackner is a coinventor of IP owned by Arizona State University (ASU) that relates to certain implementations of direct air capture. Lackner also consults for companies that work on direct air capture. ASU has licensed part of its IP to Carbon Collect and owns a stake in the company. As an employee of the University, Lackner is a technical advisor of the company and in recognition has also received shares from the company. Carbon Collect Limited also supports DAC research at ASU.

Acknowledgements

This manuscript is based upon work supported by the US Department of Energy, Office of Science, Office of Basic Energy Sciences under award number DE-SC0023343.

References

1 R. R. Bottoms (Girdler Corp.), *US Pat.*, 1783901, Separating acid gases, 1930.
2 G. T. Rochelle, *Science*, 2009, **325**, 1652–1654.
3 L. B. Gregory and W. G. Scharmann, *Ind. Eng. Chem.*, 1937, **29**, 514–519.
4 F. Goodridge, *Trans. Faraday Soc.*, 1955, **51**, 1703–1709.
5 P. Danckwerts, *Chem. Eng. Sci.*, 1979, **34**, 443–446.
6 T. L. Donaldson and Y. N. Nguyen, *Ind. Eng. Chem. Fundam.*, 1980, **19**, 260–266.
7 S. Satyapal, T. Filburn, J. Trela and J. Strange, *Energy Fuels*, 2001, **15**, 250–255.
8 K. Foo and B. Hameed, *Chem. Eng. J.*, 2010, 156, 2–10.
9 C. Gebald, J. A. Wurzbacher, A. Borgschulte, T. Zimmermann and A. Steinfeld, *Environ. Sci. Technol.*, 2014, **48**, 2497–2504.
10 J. A. Wurzbacher, C. Gebald, S. Brunner and A. Steinfeld, *Chem. Eng. J.*, 2016, **283**, 1329.
11 S. A. Didas, M. A. Sakwa-Novak, G. S. Foo, C. Sievers and C. W. Jones, *J. Phys. Chem. Lett.*, 2014, **5**, 4194–4200.
12 J. Young, E. Garcia-Diez, S. Garcia and M. van der Spek, *Energy Environ. Sci.*, 2021, **14**, 5377–5394.
13 K. S. Lackner, *Thermodynamics of the Humidity Swing Driven Air Capture of Carbon Dioxide*, Grt llc, tucson, az technical report, 2008.
14 K. Lackner, *Eur. Phys. J.: Spec. Top.*, 2009, **176**, 93–106.
15 K. S. Lackner and S. Brennan, *Clim. Change*, 2009, **96**, 357–378.
16 Y. Kaneko, *Moisture-Controlled CO_2 Sorption and Membranes Actively Pumping CO_2, 2022.*
17 T. Wang, K. S. Lackner and A. Wright, *Environ. Sci. Technol.*, 2011, **45**, 6670–6675.
18 T. Wang, K. S. Lackner and A. B. Wright, *Phys. Chem. Chem. Phys.*, 2012, **15**, 504–514.
19 X. Shi, H. Xiao, K. Kanamori, A. Yonezu, K. S. Lackner and X. Chen, *Joule*, 2020, **4**, 1823–1837.
20 Y. Kaneko and K. S. Lackner, *Phys. Chem. Chem. Phys.*, 2022, **24**, 14763–14771.
21 Y. Kaneko and K. S. Lackner, *Phys. Chem. Chem. Phys.*, 2022, **24**, 21061–21077.
22 T. Suda, M. Iijima, H. Tanaka, S. Mitsuoka and T. Iwaki, *Environ. Prog.*, 1997, **16**, 200–207.
23 P. J. Flory, *Resonance*, 2017, **22**, 416–426.
24 R. D. Raharjo, B. D. Freeman and E. S. Sanders, *J. Membr. Sci.*, 2007, **292**, 45–61.
25 G. R. Pazuki, H. Pahlevauzadeh and A. Mohseni Ahooei, *Calphad*, 2006, **30**, 27–32.
26 H. S. Harned and S. R. Scholes, *J. Am. Chem. Soc.*, 1941, **63**, 1706–1709.
27 H. S. Harned and R. Davis, *J. Am. Chem. Soc.*, 1943, **65**, 2030–2037.
28 W. G. Mook, *Environmental isotopes in the hydrological cycle: principles and applications, v. I: Introduction; theory, methods, review*, 2000.
29 R. G. Bates and G. D. Pinching, *J. Am. Chem. Soc.*, 1950, **72**, 1393–1396.
30 F. Christensson, H. C. S. Koefoed, A. C. Petersen and K. Rasmussen, *Acta Chem. Scand., Ser. A*, 1978, **32**, 15–17.
31 X. Wang, W. Conway, D. Fernandes, G. Lawrance, R. Burns, G. Puxty and M. Maeder, *J. Phys. Chem. A*, 2011, **115**, 6405–6412.
32 S. L. Clegg and P. Brimblecombe, *J. Phys. Chem.*, 1989, **93**, 7237–7248.
33 S. Pexton and E. Badger, *J. Soc. Chem. Ind.*, 1938, **57**, 107–110.

34 V. Darde, K. Thomsen, W. J. van Well, D. Bonalumi, G. Valenti and E. Macchi, *Int. J. Greenhouse Gas Control*, 2012, **8**, 61–72.
35 V. Darde, B. Maribo-Mogensen, W. J. van Well, E. H. Stenby and K. Thomsen, *Int. J. Greenhouse Gas Control*, 2012, **10**, 74–87.
36 K. Thomsen and P. Rasmussen, *Chem. Eng. Sci.*, 1999, **54**, 1787–1802.
37 K. Thomsen, P. Rasmussen and R. Gani, *Chem. Eng. Sci.*, 1996, **51**, 3675–3683.
38 C.-C. Chen, *Fluid Phase Equilib.*, 1986, **27**, 457–474.
39 D. M. Austgen, G. T. Rochelle, X. Peng and C. C. Chen, *Ind. Eng. Chem. Res.*, 1989, **28**, 1060–1073.
40 M. R. Wright, *An Introduction to Aqueous Electrolyte Solutions*, John Wiley, Chichester, England, 2007.